Monthly Notices of the ROYAL ASTRONOMICAL SOCIETY

MNRAS **460,** 2822–2833 (2016) doi:10.1093/mnras/stw1182
Advance Access publication 2016 May 18

Discovery of a long-lived, high-amplitude dusty infrared transient

C. T. Britt,[1⋆] T. J. Maccarone,[1⋆] J. D. Green,[2,3⋆] P. G. Jonker,[4,5] R. I. Hynes,[6] M. A. P. Torres,[4,7] J. Strader,[8] L. Chomiuk,[8] R. Salinas,[8] P. Lucas,[9] C. Contreras Peña,[9] R. Kurtev,[10] C. Heinke,[11] L. Smith,[9] N. J. Wright,[9] C. Johnson,[6] D. Steeghs[12] and G. Nelemans[5]

[1]*Department of Physics, Texas Tech University, Box 41051 Lubbock, TX 79409-1051, USA*
[2]*Department of Astronomy, University of Texas at Austin, 2515 Speedway, Stop C1400, Austin, TX 78712-1205, USA*
[3]*Space Telescope Science Institute, 3700 San Martin Drive, Baltimore, MD 21218, USA*
[4]*SRON, Netherlands Institute for Space Research, Sorbonnelaan 2, NL-3584 CA Utrecht, the Netherlands*
[5]*Department of Astrophysics/IMAPP, Radboud University Nijmegen, PO Box 9010, NL-6500 GL Nijmegen, the Netherlands*
[6]*Department of Physics and Astronomy, Louisiana State University, Baton Rouge, LA 70803-4001, USA*
[7]*European Southern Observatory, Alonso de Córdova 3107, Vitacura, Casilla 19001, Santiago de Chile, Chile*
[8]*Department of Physics and Astronomy, Michigan State University, East Lansing, MI 48824, USA*
[9]*Centre for Astrophysics Research, University of Hertfordshire, College Lane, Hatfield, Hertfordshire AL10 9AB, UK*
[10]*Instituto de Física y Astronomía, Universidad de Valparaíso, Ave. Gran Bretana 1111, Playa Ancha, Casilla 5030, Valparaıso, Chile*
[11]*Physics Department, University of Alberta, CCIS 4-183, Edmonton, AB T6G 2E1, Canada*
[12]*Astronomy and Astrophysics, Department of Physics, University of Warwick, Coventry CV4 7AL, UK*

Accepted 2016 May 13. Received 2016 May 12; in original form 2015 October 4

ABSTRACT

We report the detection of an infrared-selected transient which has lasted at least five years, first identified by a large mid-infrared and optical outburst from a faint X-ray source detected with the *Chandra X-ray Observatory*. In this paper we rule out several scenarios for the cause of this outburst, including a classical nova, a luminous red nova, AGN flaring, a stellar merger, and intermediate luminosity optical transients, and interpret this transient as the result of a young stellar object (YSO) of at least solar mass accreting material from the remains of the dusty envelope from which it formed, in isolation from either a dense complex of cold gas or massive star formation. This object does not fit neatly into other existing categories of large outbursts of YSOs (FU Orionis types) which may be a result of the object's mass, age, and environment. It is also possible that this object is a new type of transient unrelated to YSOs.

Key words: stars: formation – stars: pre-main-sequence – stars: variables: general – stars: variables: T Tauri, Herbig Ae/Be – stars: winds, outflows.

1 INTRODUCTION

Transient outbursts offer a unique window into astrophysics by giving astronomers access to physical changes on human time-scales. Every class of transient has been of utmost importance in understanding all areas of astronomy, from cosmology to accretion. As wide-field, time-domain surveys grow, the number of very rare events that are detected is growing correspondingly. As new transients are discovered, physical interpretation will often begin with comparisons to existing classes of transient.

Large amplitude ($\geq$6 mag) transients come from a number of physical scenarios. Classical novae (CNe) are episodes of runaway fusion of hydrogen on the surfaces of white dwarfs accreting material from a companion (Gehrz et al. 1998). These are extreme events in the optical and infrared (IR), reaching $-7 < M_V < -9$ (Yaron et al. 2005), lasting for tens or hundreds of days and sometimes producing large quantities of dust (Strope, Schaefer & Henden 2010). In these thermonuclear explosions, mass is ejected from the binary, with the amount dependent upon the mass of the white dwarf and the rate of accretion; CNe requiring less total hydrogen to set off produce less ejecta (Yaron et al. 2005). The source of material can be any companion star, from wind feeding by giants (symbiotic novae) to Roche lobe overflow from main-sequence donors in cataclysmic variables to hydrogen deficient donors leading to helium novae (Ashok & Banerjee 2003).

Another class of large amplitude Galactic transient is accretion episodes in young stellar objects (YSOs). During low-mass star formation (SF), infalling material forms an accretion disc which serves to transfer angular momentum allowing matter to fall on to the surface of the YSO. Instabilities in the disc can trigger an

⋆ E-mail: christopher.britt@ttu.edu (CTB); thomas.maccarone@ttu.edu (TJM); jgreen@stsci.edu (JDG)

episode of rapid mass accretion, in which the forming star will gain up to ≈ 0.02 $M_\odot$ in an outburst lasting many years (Herbig 1977; Hartmann & Kenyon 1996; Miller et al. 2011). Infalling envelopes are typically on the scale of 1000–10 000 au and associated with young, less evolved objects $<10^6$ yr old (Hartmann & Kenyon 1996; Sandell & Weintraub 2001; Evans et al. 2009). The mid-infrared (mid-IR) continuum is associated with reprocessed light from the circumstellar disc and envelope when present (Kenyon & Hartmann 1991). The outburst could be caused by a thermal disc instability (Bell et al. 1995), or by an interaction with another star which perturbs the disc in a gravitational instability (Bonnell & Bastien 1992).

While CNe and accretion disc instability events recur, some rarer single-event large amplitude transients can also be discovered by wide-field surveys such as the Vista Variables in Via Lactea survey (VVV; Minniti et al. 2010), the Optical Gravitational Lensing Experiment (OGLE; Udalski et al. 2008), the *Wide-field Infrared Survey Explorer* (*WISE*; Wright et al. 2010), and the Galactic Legacy Infrared Midplane Survey Extraordinaire (GLIMPSE; Benjamin et al. 2003; Churchwell et al. 2009). Dramatic, rare variables that such surveys have either discovered or revealed the nature of include stellar mergers, where a binary enters into an unstable regime of mass transfer forming a common envelope, part of which is ejected as the stellar cores inspiral and merge (Tylenda et al. 2011). The ejection of a planetary nebula could also be caught but such surveys.

Some transient classes are based on phenomenology of only a handful of objects, such as YSOs undergoing large accretion outbursts (Hartmann & Kenyon 1996). These are therefore unlikely to span the full variety of phenomena possible of a particular class of physical system (Contreras Peña et al. 2016a,b). This is true for any small sample size, but is particularly the case when the method of selection changes, as is the case here. Instead of taking a purely phenomenological approach to classifying the transient reported herein, we will consider the physical mechanisms underlying each class in order to determine if it is possible to produce the observed characteristics.

In the Galactic Bulge Survey (GBS; Jonker et al. 2011, 2014), an X-ray survey of part of the Galactic bulge conducted with the *Chandra X-ray Observatory*, we discovered a peculiar transient, CXOGBS J173643.8−282122 (hereafter CX330), where we will show in Sections 4 and 5 that the transient class which best fits the data presented in Section 3 is an accretion event in a YSO.

2 MULTIWAVELENGTH DATA SOURCES AND METHODS

While the source was discovered in optical and IR wavelengths while already in outburst, archival data in multiple wavelengths covers the region in the years before the outburst begins. In addition, the GBS collaboration took initial photometry of the bulge region prior to the X-ray observations in order to identify H α excess sources and provide a baseline for spectroscopic follow-up (Wevers et al. 2016). In addition to these early observations, we have light curves and magnitudes in multiple colours from several other surveys from after the outburst began, and have both optical and near-infrared (NIR) spectroscopy of CX330 during outburst.

2.1 Pre-outburst photometry

We use archival data from surveys of the region which are publicly available to constrain the brightness of CX330 prior to outburst, as well as a set of initial optical observations for the GBS. Several surveys cover the region to depths greater than the post-outburst brightness of CX330, yielding useful constraints on the outburst progenitor and time frame.

2.1.1 2MASS

The Two Micron All Sky Survey (2MASS; Skrutskie et al. 2006) was a ground-based survey using two 1.3 m telescopes at Mount Hopkins, AZ, and Cerro Tololo, Chile. Observations were taken in *JHK* filters. The survey depth varies with the crowding of the field. While 2MASS reaches quoted sensitivities of $K = 14.3$, in the crowded neighbourhood of CX330, we find that the cutoff sensitivity is closer to $K = 13.0$. The field was observed on 1998 July 2. No counterpart to CX330 appears in 2MASS catalogues or is visible in the images themselves.

2.1.2 Spitzer Space Telescope: GLIMPSE and MIPSGAL

Spitzer conducted surveys of the Galactic plane and Galactic bulge in NIR and mid-IR wavelengths. GLIMPSE was taken in the four IRAC filters, with effective wavelengths of 3.6, 4.5, 5.8, and 8.0 μm. Each region of the plane and bulge is covered under a different GLIMPSE survey. CX330 lies in the region covered by GLIMPSE-II, which was visited three times with exposures of 1.2 s (Churchwell et al. 2009). Multiband Infrared Photometer for Spitzer Galaxy survey (MISPGAL) covered the same region with effective wavelengths of 24 and 70 μm with the purpose, in part, of identifying all high-mass ($M > 5\,M_\odot$) protostars in the inner Milky Way disc (Rieke et al. 2004; Carey et al. 2009). The point source catalogues for GLIMPSE and MIPSGAL are publicly available.[1] We find that in the neighbourhood of CX330, the GLIMPSE point source catalogue is complete to magnitude [3.6] < 13.5, [4.5] < 13.5, [5.8] < 12.5, [8.0] < 12, and that MIPSGAL reach a depth of [24] < 8.6.

2.1.3 GBS initial optical observations

Initial optical observations for the GBS were taken in 2006 in Sloan r', i', and H α filters on the Blanco 4 m telescope at Cerro Tololo Inter-American Observatory (CTIO) with the Mosaic-II instrument, using an exposure time of 2 min. The catalogue of sources in the 12 deg^2 region is complete to $r' = 20.2$ and $i' = 19.2$, while the mean 5σ depth is $r' = 22.5$ and $i' = 21.1$ (Wevers et al. 2016). Data reduction was carried out using a pipeline created by the Cambridge Astronomical Survey Unit (CASU; González-Solares et al. 2008).

2.2 Post-outburst photometry, astrometry, and spectroscopy

2.2.1 GBS optical variability survey

We acquired eight nights of photometry, from 2010 July 8 to 15, with the Blanco 4.0 m telescope at the CTIO. Using the Mosaic-II instrument, we observed the 9 deg^2 area containing the X-ray sources identified by the first GBS X-ray observations (Jonker et al. 2011) and which contain CX330. The remaining southern GBS sources (Jonker et al. 2014) were covered in 2013 with DECam observations. Observations were made in Sloan r' with an exposure time of 120 s. Data reduction, matching variable counterparts to X-ray sources, and other optical variability results are described in detail in Britt et al. (2014).

[1] http://irsa.ipac.caltech.edu/cgi-bin/Gator/nph-scan?mission=irsa&submit=Select&projshort=SPITZER

2.2.2 VVV

The VVV survey is a time-domain survey of the Galactic plane and bulge in 2MASS filters *ZYJHK* with the VIRCAM instrument on the 4.1 m VISTA telescope located at the Paranal Observatory in Chile (Minniti et al. 2010), beginning in 2010 February and having concluded the full initial survey in 2015 October. CX330 is on VVV tile b361 at the start of VVV observations. To estimate line-of-sight reddening to the Galactic bulge, we use VVV extinction maps produced by Gonzalez et al. (2012). The K_s magnitudes of CX330 were obtained from the tile catalogues produced by the standard CASU pipeline for the VISTA/VIRCAM data. Due to the brightness of the object, the first five epochs of K_s data were saturated. To obtain reliable photometry, we measured the flux of the star in a ring with an inner radius of 0.7 arcsec and outer radius of 1.4 arcsec, thus avoiding the saturated inner core. An aperture correction was derived from non-saturated stars ($12 < K_s < 13.5$ mag) found within 1 arcmin of CX330. This procedure yields uncertainties of $\sim$0.3 mag. VVV counterparts of GBS X-ray sources are treated in detail in Greiss et al. (2014).

2.2.3 WISE and NeoWISE

WISE is a NASA satellite, launched in 2009 December, sensitive in NIR and mid-IR wavelengths in four passbands with effective wavelengths of 3.4, 4.6, 12, and 22 μm (Wright et al. 2010). Before running out of coolant and being deactivated in 2011 February, it completed an all-sky survey including two epochs of the region around CX330. In 2013 September, the satellite was reactivated and the NeoWISE survey continued in the two warmer passbands. Point source catalogues, proper motions, and images for both *WISE* and NeoWISE are publicly available through IRSA.[2]

2.2.4 OGLE-IV

OGLE-IV (Udalski, Szymański & Szymański 2015) is a time-domain optical survey of the Galactic bulge, plane and Magellenic Clouds using the 1.3 m Warsaw telescope at Las Campanas Observatory, Chile. Variability information in the field including CX330 was taken in the *I* filter with exposure times of 100 s (Udalski et al. 2012). CX330 appears in the OGLE-IV field BLG653.19 as object 81200.

2.2.5 Goodman optical spectroscopy

An optical spectrum was taken with the Goodman spectrograph on the Southern Astrophysical Research (SOAR) 4.1 m telescope on 2014 March 2 using the 400 l mm^{-1} grating centred at 7000 Å with a 1.03 arcsec slit in three 10 min exposures. It was reduced and extracted using standard packages in IRAF.[3] Two additional optical spectra were obtained with the SOAR 4.1 m telescope using the Goodman spectrograph on 2015 April 7, one moderate resolution spectrum with the same instrumental setup as before but centred at 5000 Å, and the other at a higher resolution with a 0.46 arcsec slit width and the 1200 l mm^{-1} grating centred at 6010 Å with a 10 min exposure time for an effective resolution of $R = 7200$ and binned to a dispersion of 0.6 arcsec pixel^{-1}.

2.2.6 NIR spectroscopy

An NIR *JHK* spectrum was also taken with the FLAMINGOS-2 instrument on Gemini-S in poor weather mode on 2014 March 14. The observations were made with four observations of 120 s, a six-pixel slit width, and the *HK* grism under the *HK* filter. The data reduction was performed using the UREKA package provided through Gemini Observatory which contains routines specific to the instrument. Telluric corrections and flux calibrations were performed using the A0V star HD 169257.

A second NIR spectrum was obtained with the Magellan FIRE instrument on 2015 April 28 covering the range from 0.8 to 2.5 μm with a spectral resolution of $R = 6000$. Data were reduced via the FIRE data pipeline hosted by MIT.[4]

2.3 X-rays

X-ray observations were made with the *Chandra X-ray Observatory* as a part of the *Chandra* GBS (Jonker et al. 2011, 2014). The GBS consists of many 2 ks observations covering the Galactic bulge the 12 deg^2 region $-3^\circ \leq l \leq 3^\circ$, $1^\circ \leq |b| \leq 2^\circ$, which purposefully avoids the central Galactic plane and the accompanying high extinction while preserving the high density of X-ray binaries that are the primary science target of the survey. Observations were made with the I0-I3 CCDs of the *Chandra* ACIS-I instrument (Garmire 1997). CX330 was observed in Observation ID #10015, at an off-axis angle of 6.24 arcmin and a 95 per cent confidence positional uncertainty 2.5 arcsec in radius following the methods of Hong et al. (2005). There is some overlap in GBS pointings, but CX330 does not appear on chip in any other observations. The X-ray data are discussed in further detail in Jonker et al. (2011). Matching X-ray sources to variable optical counterparts is discussed in detail in Britt et al. (2014).

3 MULTIWAVELENGTH RESULTS

CX330 began an optical and NIR outburst at some time in between 2007 and 2010. The outburst is >6.2 mag (i.e. a factor of at least 300) in the mid-IR, as the star is undetected in *Spitzer*'s MIPSGAL 24 μm band in 2006 but dominates the field in shallower *WISE* 22 μm images taken four years later (Fig. 1). A timeline of observations in different wavelengths is shown in Table 1. Because this object is variable in both optical and NIR wavelengths (Fig. 2), observations taken at different epochs should be compared with extreme caution. Even with estimated errors of the order of a factor of several, however, this object exhibits an enormous IR excess, indicating surrounding dust and gas at a cooler temperature than the central object, $T_{\rm dust} \approx 510$ K (Fig. 2).

3.1 Optical and NIR photometry before outburst

Prior to X-ray detection, GBS initial imaging showed that this object is not visible down to a limiting magnitude of $r', i' = 23$. There is a star visible inside the *Chandra* X-ray error circle in the optical and NIR images from before the outburst, but this is at an RA $= 17^{\rm h}36^{\rm m}43\overset{\rm s}{.}99$ DEC $= -28^\circ21'22\overset{''}{.}45$, which is a

[2] http://irsa.ipac.caltech.edu/cgi-bin/Gator/nph-scan?projshort=WISE&mission=irsa

[3] IRAF is distributed by the National Optical Astronomy Observatory, which is operated by the Association of Universities for Research in Astronomy (AURA) under cooperative agreement with the National Science Foundation.

[4] http://www.mit.edu/people/rsimcoe/FIRE/ob_data.htm

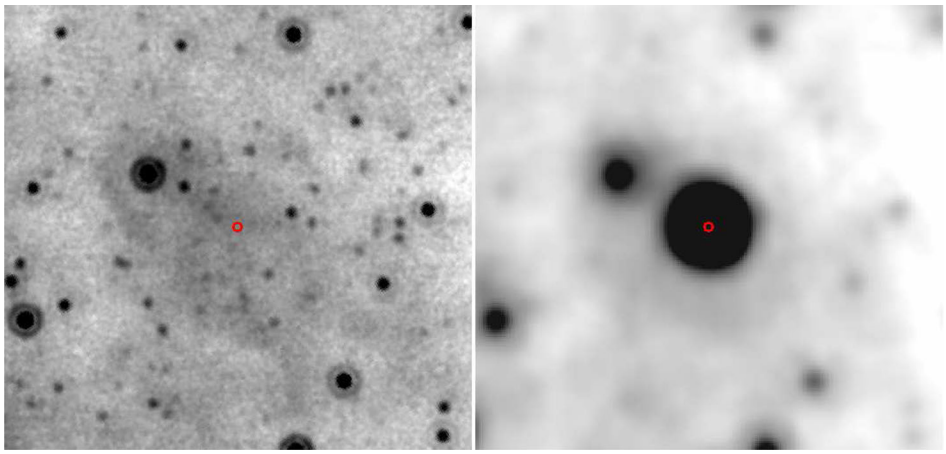

Figure 1. A comparison of CX330 brightness before and after outburst. (a) CX330 before outburst in archival MIPSGAL 24 μm images, taken on 2006 October 1. The X-ray position for CX330 from *Chandra* is overlaid in red. North is up and east is left. Each panel is 5 arcmin across. (b) CX330 in outburst in archival *WISE W4*. It is visible in all *WISE* bands, $m_{W1} = 7.72$, $m_{W2} = 6.01$, $m_{W3} = 3.32$, and $m_{W4} = 2.43$. While not visible in MIPSGAL, CX330 dominates the field in *W4*, which is especially significant considering that the MIPSGAL survey is deeper than *WISE*. As in the left-hand panel, the X-ray position from *Chandra* is overlaid in red.

Table 1. A timeline of all observations of CX330 in chronological order. A black line divides pre- and post-outburst, though it is unclear whether the X-ray observations were made before or after the outburst began. Magnitudes are in the Vega system.

Instrument	Filter	Date	Brightness
USNO-B1.0	*BRI*	1976 September 9	>19.6, >19.1, >17.4 mag
2MASS	*JHK*	1998 July 2	>14.8, >13.8, >13.0 mag
Mosaic-II	Sloan r', Sloan i', H α	2006 June 10	>23 mag
MIPSGAL	24 μm	2006 October 1	>8.6 mag
GLIMPSE	3.6 μm, 4.5 μm	2007 May 8	>13.5, >13.5 mag
	5.8 μm, 8.0 μm		>12.5, >12 mag
Chandra ACIS-I	0.3–8 keV	2009 February 4	10^{-13} ergs cm^{-2} s^{-1}
WISE	3.4 μm, 4.6 μm, 12 μm, 22 μm	2010 March 15	7.72, 6.01, 3.32, 2.43 mag
OGLE IV	*I*	2010 April 3–2012 July 10	14.6–16.3 mag
Mosaic-II	Sloan r'	2010 July 9	17.2 mag
VVV	*ZY*	2010 Sept 9–2012 June 22	14.07, 13.18 mag
	JHK		<11.5, <11.5, 10.44 mag
Flamingos-2	*K*	2014 March 14	–
Goodman	*BVR*	2015 April 7	Spectrum
FIRE	*JHK*	2015 May 4	Spectrum

different position than the transient in optical images located at RA = $17^{h}36^{m}43^{s}.88$ DEC = $-28^{\circ}21'21''.30$. The true optical/IR counterpart to CX330 is undetected prior to *WISE* observations in 2010, including in the deeper GLIMPSE ($\lambda_{\rm eff} = 3.6$, 4.5, 5.8, and 8.0 μm) and MIPSGAL ($\lambda_{\rm eff} = 24$ and 70 μm) surveys taken with the *Spitzer Space Telescope* (Carey et al. 2009; Churchwell et al. 2009). Limiting magnitudes from pre-outburst photometry are presented in Table 1.

3.2 Optical and NIR photometry after outburst

In 2010 July, a multi-epoch variability survey conducted with the Mosaic-II instrument on the Blanco 4 m telescope (Britt et al. 2014) revealed a variable counterpart with $r' = 17.2$. The GBS X-ray observations were taken in between these optical observations on 2009 February 4. In 2010 observations, CX330 shows aperiodic flickering over a range of 0.3 mag, with the largest intranight variations of 0.15 mag. The X-ray to optical flux ratio, before correcting for extinction, was estimated to be $F_X/F_{r'} = 10^{-0.9}$, which drops to $F_X/F_{r'} = 10^{-2.8}$ with extinction for the line of sight to the bulge as measured by Gonzalez et al. (2012), and drops further with any local extinction. In DECam observations in 2013, taken over two nights with an average sampling of 15 min, CX330 also appears at $i' \approx 17.45$ as a variable with smooth, aperiodic variability in on the time-scale of hours, with intranight variations of 0.15 mag.

OGLE-IV shows CX330 as an irregular variable (Udalski et al. 2012) with flickering and a very slow decay time over the observational period. The light curve, along with Mosaic-II, DECam, VVV, and *WISE* and NeoWISE observations, is shown in the right-hand panel of Fig. 2.

CX330 is at least 7 mag brighter in *W1* ($\lambda_{\rm eff} = 3.6$ μm) than in the GLIMPSE IRAC 3.4 μm band, and at least 6 mag brighter in *W4* ($\lambda_{\rm eff} = 22$ μm) than in MIPSGAL 24 μm images.

3.3 Astrometry

The proper motion and parallax of CX330 were fitted independently in the $\alpha\cos\delta$ and δ dimensions using a robust technique involving an iterative reweighting of data points as a function of their residuals. We used the 108 *Ks* band epochs with seeing <1.2 arcsec of VVV

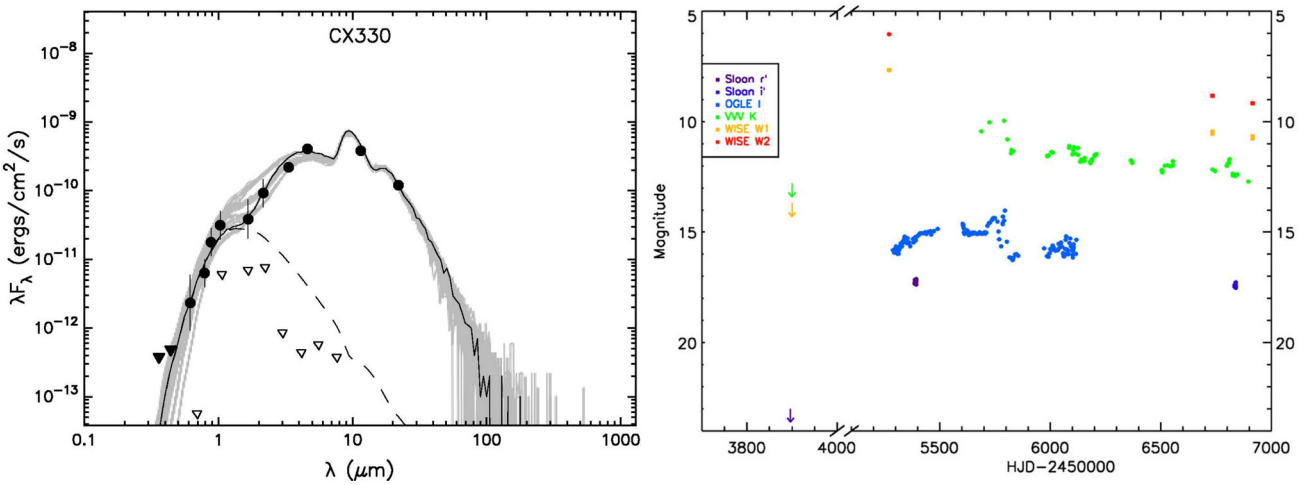

Figure 2. SED and light curve of CX330. (a) An SED of CX330 fitted with a variety of YSO models(Robitaille et al. 2007). The dotted line represents a reddened single temperature blackbody. Open triangles are upper limits from photometry before the outburst began. Because CX330 is variable while in outburst, the comparison of data at different epochs is dubious, and we therefore have included error bars that reflect the amplitude of variability observed in each bandpass for observations taken after the *WISE* data. The modelling clearly demonstrates that a large, cooler dusty envelope around the central hot source is necessary to fit the IR excess. (b) Available light curves of CX330 since 2010. Upper limits are provided where available.

tile b361 available to us as of 2014 April 30, a total epoch baseline of 2.9 yr. We selected 97 references sources from within 62 arcsec of the target through an iterative rejection of sources with significant proper motion. We measure a total proper motion relative to the reference sources of 1.6 ± 3.3 mas yr^{-1} and a parallax of 2.8 ± 2.5 mas. The proper motion components are 1.2 ± 2.6 and 1.0 ± 2.0 mas yr^{-1} in $\alpha\cos\delta$ and δ, respectively, and parallax components are 2.5 ± 2.5 and 44.6 ± 28.4 mas in $\alpha\cos\delta$ and δ. The final parallax is the average of the two measurements weighted by the reciprocal of their uncertainty squared, resulting in a value of 2.8 ± 2.5 mas.

3.4 Optical and NIR spectroscopy

The optical spectrum taken in 2014 shows narrow emission lines which we used to measure the radial velocity of CX330. The heliocentric radial velocity we measure to be 60 ± 15 km s^{-1}, where the uncertainty is dominated by the wavelength calibration of the spectrum.

The lower resolution spectrum of 2015 covers H β but the extinction is high enough to quench it completely, despite the large H α line, while the nearby broad [O III] doublet at 4959 and 5007 Å is still present with $F([\mathrm{O\ III}\ 5007])/F(\mathrm{H}\,\beta) > 20$, suggesting either very high intrinsic $I([\mathrm{O\ III}\ 5007])/I(\mathrm{H}\,\alpha)$ values or that the [O III] lines are produced in a region separate from the Balmer emission.

We can use the Balmer decrement to measure the reddening to the source (Osterbrock 1989):

$$E(B-V) = \frac{2.5}{k(\mathrm{H}\,\beta) - k(\mathrm{H}\,\alpha)} \log \frac{\mathrm{H}\,\alpha/\mathrm{H}\,\beta_{\mathrm{obs}}}{\mathrm{H}\,\alpha/\mathrm{H}\,\beta_{\mathrm{int}}},$$

where $k(\lambda)$ is the extinction coefficient at that wavelength for a given extinction law. We place a lower limit on the observed ratio H α/H β > 280, which for an intrinsic ratio of H α/H $\beta \approx 3$ and taking $k(\mathrm{H}\,\beta) - k(\mathrm{H}\,\alpha) = 1.25$ for the Milky Way (Seaton 1979) gives $E(B-V) > 4.1$. Using other extinction laws with lower values of $k(\mathrm{H}\,\beta) - k(\mathrm{H}\,\alpha)$ found in the literature drives the reddening up higher. We use the highest value found in the literature as a conservative lower limit on $E(B-V)$. Even with this conservative assumption, however, this is much higher than the line of sight extinction measured in the VVV survey (Gonzalez et al. 2012), $E(B-V) = 2.06 \pm 0.23$ following the extinction law of Cardelli, Clayton & Mathis (1989). This leaves $E(B-V) > 2$ remaining to local extinction. If this object is in front of the Galactic bulge, this lower limit moves up, while moving beyond the bulge in this line of sight adds no substantial foreground reddening as the radius from and height above the centre of the Galaxy continue to increase well above a scaleheight of the disc. We can therefore firmly conclude that the extinction responsible for quenching H β is local.

The [N II] lines in 2015, >5 yr after the outburst begins, are substantially weakened compared to 2014, with [N II 5755] ∼4 × fainter than [C IV 5805], when they were of roughly equivalent strength.

Each epoch of optical spectroscopy of CX330 (Fig. 3) shows strong hydrogen emission, as well as He I emission. The lines are not redshifted beyond the typical dispersion of stellar velocities in this line of sight, which rules out an extragalactic origin. Also present are strong, high ionization state forbidden lines, most notably [O III] 4959+5007 Å and [N II] 5755 Å. O I 6300 Å and other O I lines are absent. The forbidden emission lines are very broad, with a full width at half-maximum (FWHM) of 1400 km s^{-1}, which for a spherical outflow would imply an expansion velocity of 700 km s^{-1}. The allowed transitions of hydrogen and helium in 2014 have cores that are much narrower, with an FWHM of <140 km s^{-1}, with a broad pedestal as wide as the forbidden lines. In 2015, this central emission core fades and leaves a broad base with a double peaked profile with peaks at $v = -170$ km s^{-1} and +260 km s^{-1} with a core blueshifted by 25 km s^{-1} relative to the line centre, with the blue peak suppressed compared to the red, a common line profile of bipolar outflows.

The NIR spectrum shows strong Brackett and Paschen emission in addition to He I emission lines. The flux calibrated continuum is poorly fit by a single blackbody with extinction, and a second large cool component is necessary to fit the *K*-band flux which increases moving to longer wavelengths.

The FIRE spectrum taken in 2015, shown in Fig. 4, shows strong Brackett and Paschen series emission as well as both He I and He II, Fe II, and C IV and C III. The velocity profiles of the helium and hydrogen lines is the same as that of H α in 2015 shown in Fig. 3,

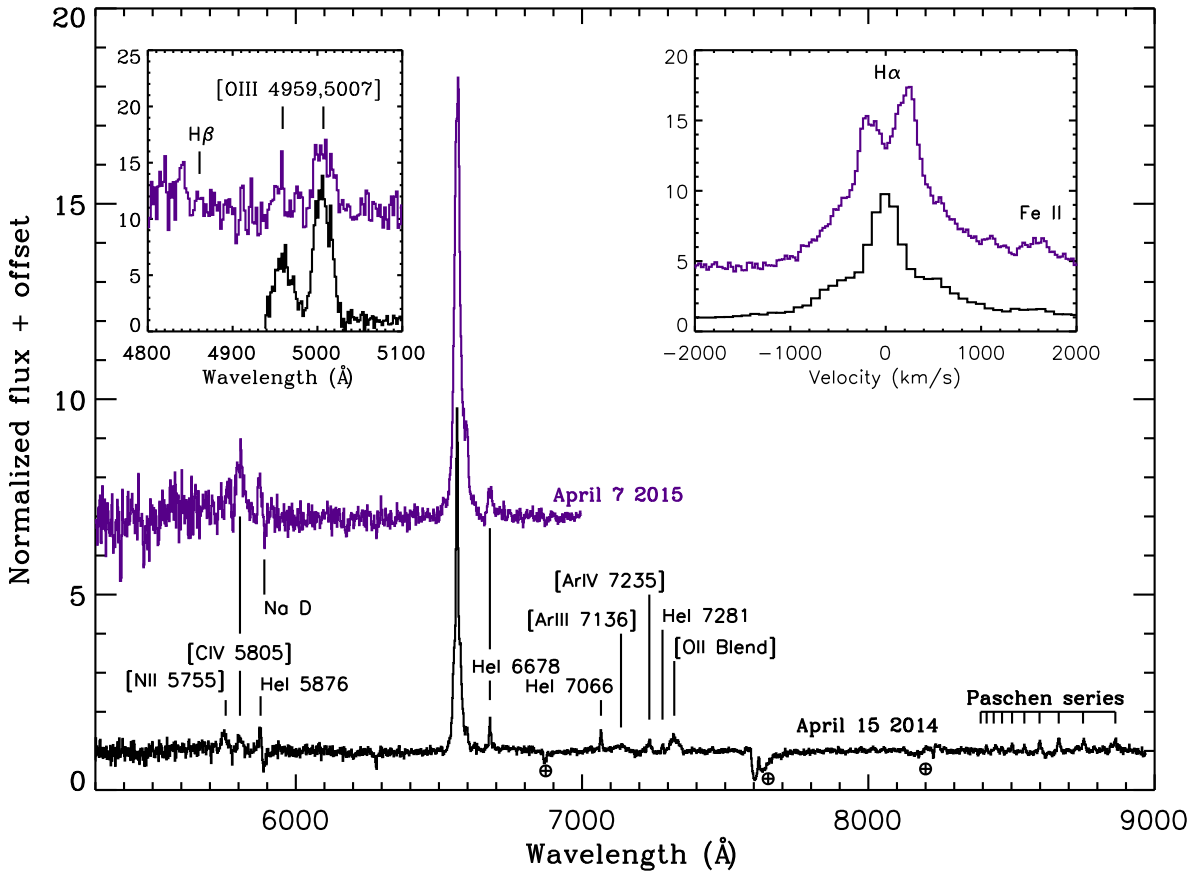

Figure 3. Optical spectroscopy of CX330 in 2014 (black) and 2015 (purple), normalized to continuum with an arbitrary offset added. Telluric lines are marked with ⊕. The presence of [O III] is notable because it requires a strong UV ionizing flux above 35.1 eV to ionize O^{+} and produce O^{++} or comparably high shock temperatures especially since the neutral oxygen feature [O I] at 6300 Å is absent. In 2014, the forbidden emission lines are also much broader than the core hydrogen and helium features, though there is a broad pedestal at the base of H and He lines that shares the same velocity profile as the forbidden lines.

while the Fe II lines are decidedly more flat topped, with a full width at zero intensity (FWZI) of 990 km s^{-1}. Some of the hydrogen lines such as Pa β and Br γ have FWZI measures ∼2000 km s^{-1} but are also contaminated with He I and He II lines which are present and are broadening the observed base. The amalgamation of light from distinct shock regions in different radial directions from the source and as [O III] regions cool and begin producing hydrogen recombination could also artificially broaden the lines. Similar to the 2014 FLAMINGOS-2 NIR spectrum, CO and water lines are also absent in this spectrum.

3.5 X-ray observations

We first identified CX330 as an X-ray source with and X-ray flux $F_X \approx 6 \times 10^{-14}$ ergs cm^{-2} s^{-1} at a position 2° above the Galactic mid-plane. The initial 2 ks X-ray observations are described in detail in Jonker et al. (2011). In this observation, CX330 has eight counts above background, a highly significant point source for *Chandra*'s background in the short exposure time. At an off-axis angle of 6.24 arcmin the pileup for eight photons in 2 ks is negligible. The X-ray luminosity in 2009 is $\approx d_{\rm kpc}^2 \times 2 \times 10^{30}$ ergs s^{-1}. The optical/IR counterpart for CX330 is 0.8 arcsec from the *Chandra* X-ray position, well within the 95 per cent confidence region for the X-ray observation (Jonker et al. 2011; Britt et al. 2014). While there are so few counts that a wide variety of models can adequately fit the data, they do offer a few constraints. First, there are no photons below 1 keV. Even with very high extinction, it is difficult to have a very soft X-ray spectrum with kT < 0.5 keV such as a super soft source without also having an implausibly high intrinsic X-ray luminosity in order to provide harder photons while killing the softer ones. The lack of photons below 1 keV gives a range of $N_{\rm H}$ that is consistent with the extreme absorption seen in the optical wavelengths, which is suggestive that the dust around the system was present at time of X-ray observations. We stress, however, that with only eight photons, many different models can fit the X-ray spectrum and a wide range of values is allowed for photon index and $N_{\rm H}$.

4 INTERPRETATIONS OF THIS TRANSIENT

This object is very unusual in several respects, so we take the opportunity here to rule out some interpretations and reconcile some differences with known classes.

4.1 AGN

A 3σ upper limit on the redshift of $z < 0.0003$ based on the hydrogen emission lines in 2014 means that the source must be quite nearby in cosmological scales, yet no galaxy is resolved in any wavelength. We conclude that CX330 is of Galactic origin. A tidal disruption event around a supermassive black hole (or even around an intermediate mass black hole in a globular cluster) is ruled out for the same reason.

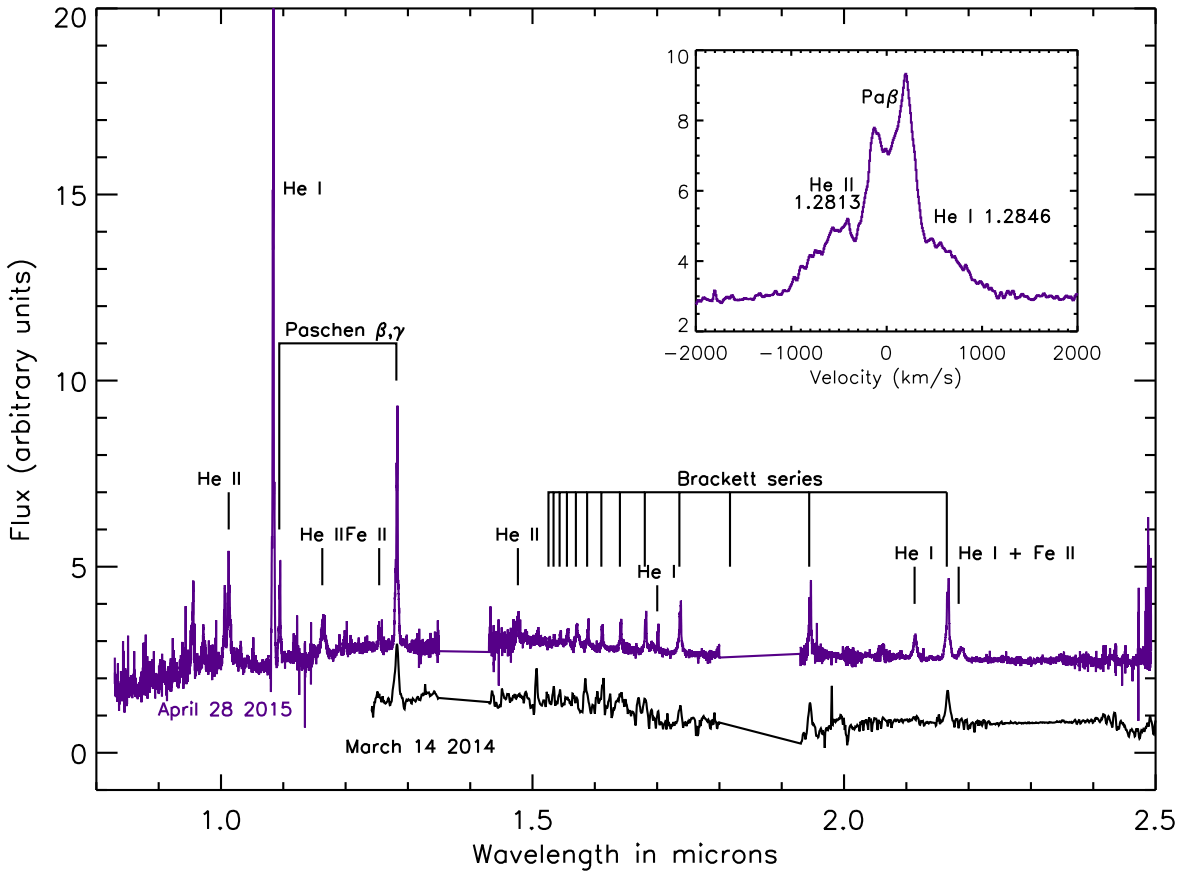

Figure 4. NIR spectra of CX330. The first IR spectrum obtained with FLAMINGOS-2 in 2014 March is plotted in black. This observation was taken in poor weather, leaving a noisy spectrum. The widths of the spectral lines in this observation are dominated by the low instrumental resolution. A second spectrum obtained with the FIRE instrument on the Magellan telescope in 2015 May at much higher resolution, plotted in purple, shows many lines of hydrogen and helium in emission, including He II. Many of the stronger hydrogen lines are not isolated, but are blended with lines of He I and He II.

4.2 Classical nova

CNe exhibit a wide variety of phenomenologies, and require careful consideration. We disfavour this interpretation for the following reasons.

4.2.1 Dusty at late times

CX330 remains heavily obscured, with a strong IR excess, years after outburst. In a nova scenario where the dust is produced in an expanding shell, as in the nova V1280 Sco (Naito et al. 2012) or Nova Mon 2012 (Munari et al. 2013), the dust expands with the nova shell and results in reddening lessening over time (Hachisu & Kato 2014). In CX330, the reddening measured from $K - I$ remains constant, or is even growing, over years, which suggests that the local dust is either not associated with the outflow or that dust is somehow being continuously generated from a nova even after the nebular phase has begun. While some evolved stars generate copious amounts of dust, we can firmly rule out a symbiotic nova with a donor from the asymptotic giant branch to most of the red giant branch (RGB) based on the pre-outburst upper limits even taking into account the large amount of reddening observed. We can hide at a distance of the Galactic bulge less evolved stars at the start of the RGB only by assuming that all of the copious local reddening above that in the line of sight to the Galactic bulge ($E(B-V) \geq 2$) is present locally before the outburst begins; however, RGB stars typically have mass-loss rates from wind from 10^{-9} to 10^{-5} $M_{\odot}$ yr^{-1}, with higher rates only possible for the more evolved, luminous stars which we can rule out firmly, and the others do not produce material in anywhere close to sufficient quantities to provide the observed reddening to this object.

4.2.2 The long decay time-scale of CX330

The outburst of CX330 lasts >5 yr and is ongoing at the time of writing, decaying only ∼3 mag in that time. It is unclear whether or not OGLE-IV observations catch the peak of the outburst. This area is covered by All Sky Automated Survey (ASAS) down to $I = 14$ until 2009 October 26, so an outburst peak could be hidden while CX330 is behind the Sun from 2009 November–2010 February. Most CNe dim much faster from peak than CX330 does (assuming that the peak is observed), decaying several magnitudes on a time-scale of weeks to months (Strope et al. 2010), originating from much smaller spatial scales than those in YSOs. Even if the peak of the outburst is unobserved, this light curve remains unusually slow for a nova. Some rare CNe, however, can proceed much more slowly and form large amounts of dust which regulates the brightness of the novae through the optical depth (Chesneau et al. 2008). Objects like V1280 Sco have a long plateau phase after dust production that lasts years, but there is no high frequency variability in this phase (Naito et al. 2012) while observations of CX330 with DECam in 2014 show rapid variability on the time-scale of a day or less even four years after the outburst begins and while its spectral energy

distribution (SED) peaks in the NIR. Also, there is a fairly well defined relationship between the outflow speed of a CN, $v_{\rm out}$, and the decay speed, t_3 (Esenoglu et al. 2000). While novae can have a variety of light-curve morphologies (Strope et al. 2010), the scatter this may introduce into the relationship between $v_{\rm out}$ and t_3 is much less than the deviation of CX330 in comparison if we assume that the peak of the outburst is observed in OGLE-IV (see fig. 3 of Esenoglu et al. 2000). Not only do no CNe known have t_3 as long as CX330's now is, 2100 d measured in *I* band, but those few that do have t_3 > 1 yr have outflow speeds of only a few tens of km s^{-1} (Warner 2003). This argument only applies to the case that we observe the outburst peak, otherwise we have no starting point with which to measure t_3.

4.2.3 *Nova returning from dust dip requires fine tuning*

One possibility considered that avoids the problem of t_3 versus $v_{\rm out}$ discussed above is that the outburst we observe is not the initial nova, but the recovery from a dust dip as in D class novae (Strope et al. 2010). However, in this case the eruption time and duration of a CNe must be fine-tuned to avoid detection in all-sky surveys.

In D class novae, the dust dip lasts for 100–200 d, with those novae generating more dust having longer dips. If the small rise seen at the start of OGLE observations is a recovery from a dust dip, then the nova eruption must have occurred in the 100–200 d prior to *WISE* observations on 2010 March 15, likely closer to 200 d given the large amount of reddening observed. The gap between ASAS and OGLE observations leaves 141 d for CX330 to nova while it is behind the Sun and return from a dust dip. This is not a short enough time to absolutely rule out a D class nova eruption on its own, but it does require that the nova go off within a month of ASAS observations stopping and that the duration is unusually short for the amount of dust generated.

4.2.4 *Variability at late times*

The variability at late times seen in CX330 is uncharacteristic of D class nova. The *I*-band light curve in OGLE IV is smooth for over a year, with a possible rebrightening while behind the sun between MJD 55500 and 55600. There are observed rebrightenings lasting 1–2 months in the second year of observations, which then remains flat until halfway through the third year of observation when variability on time-scales of days begins.

It is not uncommon for novae to rebrighten after the initial eruption (Strope et al. 2010). These 'jitters', however, follow similar patterns; they start before the nova enters the nebular phase and the time between them grows logarithmically with time since the start of the outburst (Pejcha 2009). Because they are likely caused by sudden changes in the hydrogen burning rate in a white dwarf envelope, they occur on massive white dwarves in fast novae (Pejcha 2009). Any slow nova, as late dusty novae must be (Williams et al. 2013), must originate on a low-mass white dwarf. The rebrightenings seen in fast novae are therefore not a viable explanation for the late time variability.

4.2.5 *Estimate of ejecta mass required*

In the finely timed scenario of a D-class dust-dip nova discussed above (Strope et al. 2010), we can use the lower limits on reddening along with the outflow speed and time since eruption to make a crude estimate of the mass of the ejecta.

For a nova in the bulge at 10 kpc experiencing the full amount of interstellar reddening (Gonzalez et al. 2012), the remaining local extinction amounts to $E(B-V) > 2.0 \pm 0.6$. Assuming average interstellar gas-to-dust ratios, the column density from local sources is $N_{\rm H} = 5.6 \times 10^{21}$ atoms cm^{-2} $\times$ $E(B-V) > 1.1(\pm0.3) \times 10^{22}$ atoms cm^{-2}. In a nova scenario where the absorbing material is generated in an outflow started at the time of the eruption, the material is at a radius of $R \approx 1000$ au from the nova after five years given the observed velocity widths. Assuming that all of the Balmer emission is behind all of the mass as a lower limit to the amount of mass in the ejecta required to achieve the reddening seen, we still require $\approx$0.01 M$_\odot$ to generate the required column density five years after an outburst moving at the observed speed. This is orders of magnitude higher than the most massive nova ejecta, which themselves require low accretion rates and therefore occur very infrequently (Yaron et al. 2005). We stress again that the limit on local $E(B-V)$ from spectra is conservative in two respects: H β is assumed to be just below the detection threshold when it may be fainter and we use the most conservative extinction law we could find (Seaton 1979). It seems certain, therefore, that a single nova event is incapable of producing the observed amount of dust, while dust from past novae should be ejected by the binary before recurrence.

4.2.6 *Spectral evolution*

At first glance, the emission line profile in 2015 is a much narrower version of the P Cygni profiles seen in the nova V1280 Sco only two weeks after the eruption (Das et al. 2008) or the spectrum of the nova KT Eri taken only 17 d after eruption (Munari, Mason & Valisa 2014). The high order Paschen and Brackett lines are very strong, meaning the density is high in the region where these lines are being produced.

However, this spectrum was taken >4 yr after the outburst began. At the expansion velocity of the forbidden lines, a nova shell should have expanded $\gtrsim$600 au, which makes it difficult to envisage any nova scenario maintaining a sufficient density to explain the strong Paschen lines (Raj et al. 2015). The late epoch spectra resemble some novae at early times, yet the colour of CX330 remains roughly constant, or even reddens, with time (Fig. 2). In dust producing novae, the broad-band colours generally become bluer with time as the optical depth of dust drops over time (Hachisu & Kato 2014). We conclude from the constant (or slight reddening) colour that the local dust cloud around CX330 is not expanding, but may be cooling.

4.2.7 *Helium nova*

Helium novae (fusion of helium on the surface of a white dwarf primary) can be very red and long lasting, but are hydrogen deficient by definition (Woudt & Steeghs 2005). CX330 shows very strong hydrogen lines, ruling out this interpretation.

4.2.8 *Symbiotic recurrent nova*

Symbiotic novae can last years or decades, with dust that is not as quickly ejected from the wider system. While this could explain the constant reddening seen in CX330, dust still needs to be local to the system before outburst to hide the donor star, and the donor star must still be low on the RGB. Since winds from such stars are inadequate to produce this dust, we here consider a recurrent nova

(RN) in which the ejecta do not have time to fully dissipate before another eruption renews the dust. While there is no evidence of a giant companion in the spectra, it is clear from the magnitude of the outburst that any companion present cannot contribute a significant portion of the light at any wavelength. However, RNe require high-mass white dwarfs in order to trigger a nova with less material on the surface. To produce $\gtrsim 10^{-2}$ $M_{\odot}$ of dust around the binary when RNe eject of the order of 10^{-5}–10^{-6} $M_{\odot}$ in an eruption requires the material of $\gtrsim 10^{3-4}$ eruptions over $\gtrsim 10^{4-6}$ yr. We consider that the dust from novae many thousands of years ago cannot remain local enough either to be heated to >500 K as suggested by *WISE* colours or to provide the optical depth observed.

4.3 Luminous red nova

This class has become much better understood in the last 10 years and is likely a misnomer unrelated to CNe. The favoured interpretation is that they are the result of stellar mergers (Tylenda et al. 2011). Though the IR emission can last longer, the optical light, with some exceptions, fades in a matter of weeks to months, much faster than is observed in CX330. More importantly, the absolute magnitudes of these events are quite bright, and would place CX330 well beyond the bulge either in the Galactic halo or even outside of the Galaxy. Several progenitor scenarios suggest that they have giants as precursors, whereas CX330 is undetected in deep observations in optical and IR wavelengths before the outburst began. Also, a giant precursor makes the large outflow velocity much harder to achieve since they have much lower escape velocities than main-sequence stars. For mergers of main-sequence stars, the time-scales are much shorter than those for giants, e.g. the merging contact binary V1309 Sco (Tylenda et al. 2011), and makes the length of the outburst difficult to achieve.

Perhaps a region of parameter space exists where a merger between a subgiant and brown dwarf companion could be long lived and faint compared to the usual transient types. This scenario requires careful simulation to totally eliminate, but seems fine-tuned.

4.4 Accretion driven outburst in a YSO

4.4.1 Spectroscopy

The optical and IR spectra are unusual for YSOs in outburst, consisting of emission lines on a hot, featureless continuum. As discussed in Section 3.4, the nebular emission lines are broad in each observation, while the allowed hydrogen lines transition from being narrow and single peaked with a broad base to broad and double peaked, with the blue peak suppressed relative to the red. This is a profile commonly seen in bipolar outflows (Steele et al. 2011). The separation between peaks observed in the H α profile in 2015 is an order of magnitude higher than one would expect from a Keplerian disc at au scales. In the YSO interpretation, then, we will more closely examine the case that a bipolar outflow is responsible for the double-peaked feature as a Keplerian disc does not fit. Bipolar outflows are a common feature of accreting systems, and are limited in velocity to roughly the escape velocity of the region from which they are ejected (Livio 1999). If we assume an accretion rate comparable to the most extreme YSO transients, FU Orionis objects (FUors), and a compactness corresponding an escape velocity of the outflow speed observed, then it is clear that the accretion temperature is not hot enough to photoionize [O III].

Another way to produce high ionizations is through shocks, which occur when fast-moving material encounters slower material and collides (Osterbrock 1989). The shock temperatures corresponding to the observed outflow velocities are high enough to produce these lines (Osterbrock 1989). We therefore find that [O III] and other high ionization lines in this scenario are produced in a shock from an outflow, from a wind or jet ploughing into what is left of the cooler envelope of gas feeding the SF. A central object massive enough to generate [O III] or He II through photoionization should be visible in pre-outburst photometry even at bulge distances, as discussed in further detail below. We envisage that the high ionization states are a result of this shock rather than from photoionization from the central source. The velocities observed are higher than in most other YSOs and can be explained by having a more compact or more massive central object. The higher velocity outflow then gives a hotter shock region. As the shock propagates and cools, hydrogen can recombine which would explain the broader line profiles in recombination lines in 2015 compared to 2014 as the shock regions begin to dominate the emission. Since shocks can be produced in many locations which we do not resolve, the velocity distribution may be artificially broadened by thermalized gas shocking in different radial directions from the central source.

Lithium absorption at $\lambda\lambda = 6707$ Å is a common feature of YSOs, though our observations are of too low a signal-to-noise ratio to expect to detect this line. Our 1σ upper limit for the equivalent width of Li 6707 is EW < 0.2, which is not discriminating for YSOs, for which EW = 0.1–0.2 Å is not unusual. This also does not account for shielding of the line by an elevated continuum, which must be present in CX330 since the continuum at time of spectroscopy is at least 300 times brighter than the base level of the photosphere.

The X-ray spectrum, such as it is, is consistent with that of eruptive YSOs such as FUor (Skinner et al. 2010), which consist of two components, one hard ($kT \approx 3$–4 keV) and one soft ($kT < 1$ keV) thermal component with high absorption ($N_{\rm H} \approx 10^{23}$), though with only eight photons we stress that many other models are also consistent with the available X-ray data.

The absence of absorption lines in any part of the spectrum, particularly the CO lines at 2.3 μm, is inconsistent with the previously largest class of YSO outbursts, the FUor class, but could be explained with a hotter accretion disc than is seen in those objects. The FUor class has been described using a small number of objects, and are only one manifestation of the broader class of 'eruptive YSOs', which includes objects that sometimes do not show CO absorption. Indeed, as the sample of eruptive YSOs grows, it is becoming clearer that many objects do not fit neatly into the FUor or smaller, shorter EX Orionis class, but contain some characteristics of both (Contreras Peña et al. 2016a). It is also important to note that we do not detect the stellar photosphere in any observations; the outburst is so large that the light is completely dominated by some combination of the accretion disc, reprocessing from the dusty envelope around the system, and shocks associated with the outflow. This makes it extremely difficult to precisely constrain the stellar properties.

4.4.2 Isolation and presence of interstellar dust

In the YSO interpretation, the most interesting characteristic of CX330 is its position on the sky. It is 2° above the Galactic plane, and well outside of any known star-forming region. All known large magnitude outbursting YSOs such as FUors are located in star-forming regions, likely in part because of selection biases but the actual distribution is also concentrated in these regions (Contreras

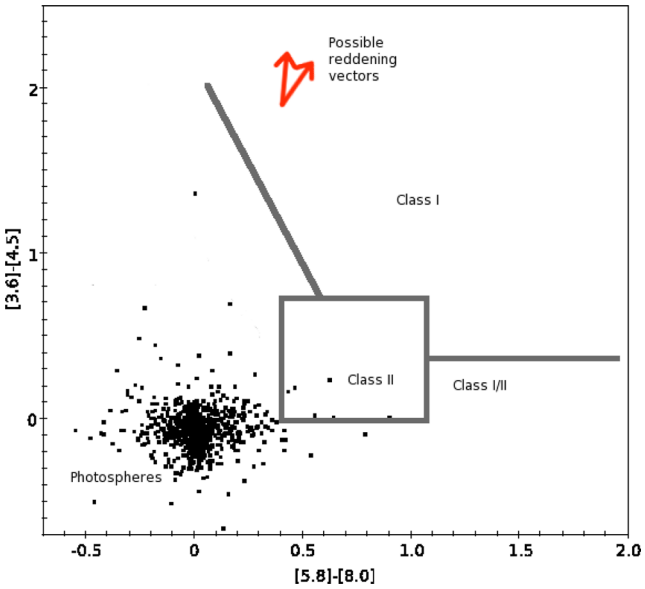

Figure 5. The *Spitzer* GLIMPSE point source catalogue contains no population of protostars within 2 arcmin of CX330. Using criterion to select YSOs in the IRAC colour–colour map (e.g. Qiu et al. 2008; Robitaille et al. 2008), we find no evidence of a cluster of star formation in this region. Before outburst, CX330 was not detectable in GLIMPSE limits, which could be true of most stars later than A0 spectral type at most likely distances and all O stars at any distance.

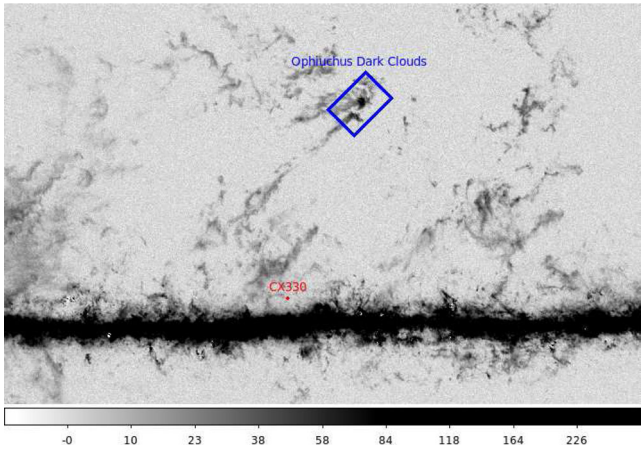

Figure 6. The type 3 CO map of the Galaxy produced by the *Planck* satellite shows that there is no prominent SF region at this location. A nearby region of SF, the ρ Ophiuci cloud complex, is highlighted to aid comparison of CO around CX330 with that around star-forming regions. For scale, the distance of CX330 above the Galactic plane is 2°.0.

Peña et al. 2014, 2016b). Additionally, CX330 must have formed *in situ*, since its measured proper motion with the VVV survey has an upper limit of 3.3 mas yr^{-1}. The phase of stellar evolution in which disc instability events occur is generally thought to be within 10^6 yr after the formation of the disc (Hartmann 1998) so that it can have drifted less than a degree since the time of formation. Upper limits on the parallax angle from VVV astrometry place a lower limit on the distance of 350 pc. Distances near the Galactic bulge, on the other hand, are also unlikely because then that would imply an X-ray luminosity of $L_X \approx 5 \times 10^{32}$ ergs s^{-1}, two orders of magnitude more luminous than FUor itself, which has $L_X \approx 6 \times 10^{30}$ ergs s^{-1} (Skinner et al. 2010). A distance of ∼1–3 kpc is consistent with the X-ray brightness observed, the lack of observed proper motion, and the lack of optical or IR detection prior to outburst. A height of 2° above the disc at 2 kpc translates to a height above the disc of 36 pc, which is within the scaleheight of gas for the Milky Way which is ∼100 pc.

Because the progenitor of CX330 is not seen in observations prior to its outburst, it is entirely possible that other intermediate to low-mass stars exist in its immediate vicinity. We can place upper limits on the stars around it from existing catalogues and our own data from before the outburst began. All OV and B0V should be detected all the way to the Galactic bulge with $E(B-V) = 4$ (the line-of-sight reddening is only $E(B-V) = 2$ at the bulge, but we include a substantial fudge factor for local dust that may shroud other systems). At a distance of 3 kpc, which includes two spiral arms, we would expect to see all OV and BV stars associated with CX330. For a distance of 1 kpc, we would also expect to see early A stars. If reddening is less than $E(B-V) = 4$ for associated stars then cooler objects would also be visible. Using archival Spitzer point source catalogue within 2 arcmin of CX330, no obvious young stars are visible, as shown in Fig. 5. It seems likely, therefore, that no high-mass SF is taking place associated with CX330. While CX330 cannot be placed on Fig. 5 directly since it does not appear in the GLIMPSE catalogue, using the *WISE* colours ($W1 - W2 = 1.7$, $W2 - W3 = 2.7$) and the classification scheme of Koenig & Leisawitz (2014) places CX330 on the border between class I and class II YSOs. It is unsurprising that intermediate and low-mass YSOs in the region are not visible in GLIMPSE catalogues as CX330 itself was below detection limits prior to outburst.

To estimate the amount of gas and dust in the region we use the dust maps from the *Planck* mission (Fig. 6; Planck Collaboration XIII 2014). These yield a column density of molecular hydrogen of 5×10^{20} cm^{-2}, which is ∼1000 times lower than the column densities around the locations of known large outbursts of YSOs and ∼10–20 times lower than the column density at which a cloud should become unstable to gravitational collapse (André et al. 2010). CX330 therefore cannot reside in a cloud as large as a pixel of the *Planck* maps on the sky (∼3 arcmin). The typical angular size of a Bok Globule at 1 kpc would be of order 1 arcmin, while larger, more diffuse complexes would typically occupy a few square degrees. No such globule is seen in optical or NIR images of the area, though there is diffuse dust typical of lines of sight at this latitude. In 24 μm *WISE* and MIPSGAL images, this dust is warm and glowing, though this does not mean that the same would have been true 10^6 yr ago. CX330 appears within 2 arcsec of the geometric centre of the warm dust which is roughly 2 arcmin × 1 arcmin in area, though CX330 lies at the western edge of the area of higher optical extinction. There may be no real association between CX330 and this dust cloud, but this possibility merits further study. As SF occurs on the order of dynamical times (Elmegreen 2000), faster at small scales, the rapid collapse of a turbulent cloud of gas could proceed within 10^6 yr for a small enough cloud.

The 'Handbook of Star Forming Regions' lists no star-forming regions within 3 deg of CX330. The nearest is NGC 6383, which is at $l = 355.7$, $b = 0.0$, making it about 4 deg away. The most prominent regions in this direction are the Pipe Nebula and the B59 star-forming core (∼8° away) and the Corona Australis region (∼17° away). Both of these regions are relatively nearby, at distances ≈130 pc, making them unlikely to be associated with this object. The latter region is also quite isolated and offset from other molecular material. Beyond those structures, the majority of star-forming regions at these Galactic longitudes are located in the

Scutum–Centaurus spiral arm of our galaxy, which is about 2–3 kpc from us. There are many prominent H II regions and star-forming regions in this arm, including the Eagle Nebula and the Lagoon Nebula (and NGC 6383 above), but there is a notable absence of such regions in the vicinity of CX330.

The CO map presented in Fig. 6 is the type 3 CO discovery map produced by the *Planck* satellite, which combines CO line ratios and models of the cosmic microwave background, CO emission, synchrotron and free–free emission to identify faint molecular clouds (Planck Collaboration XIII 2014) with a resolution of 5.5 arcmin. In order to ascertain how isolated CX330 is compared to YSOs with large outbursts, we compare the velocity-integrated CO distribution of the sky within 30 arcmin of CX330 to that near eight known FUors (they being the most extreme class of outbursting YSO yet found), all associated with the giant molecular clouds (GMC) of Cygnus or Orion. Every FUor, without exception, has an associated region of dense CO gas well above the *Planck* background reaching anywhere from 35–100 $K_{\rm RJ}$ km s^{-1}, while the most CO around CX330 is 15 $K_{\rm RJ}$ km s^{-1}. The CO concentration at the position of CX330 is also much less than at known FUor stars at 7 $K_{\rm RJ}$ km s^{-1}. The closest any FUor gets is FUor itself at 13 $K_{\rm RJ}$ km s^{-1}, though it lies at the edge of a much denser region while CX330 does not.

At least one other flaring YSO has been detected outside of a star-forming region, GPSV15 (Contreras Peña et al. 2014), though it is unclear how old this object is or if it is still accreting material.

The neighbourhood around CX330 in the *WISE* catalogues reveals only one other object with an IR excess, which is not as red as CX330 and is 5 arcmin away. There are a few objects with red *W*2–*W*3 adjacent to CX330, but these are not visible in images and are likely due to the wings of the profile of CX330 in *W*3, which is quite spatially extended. This may not indicate a lack of nearby low-mass YSOs, however, as CX330 was itself undetectable outside of outburst. In *WISE* images, only warm dust is visible which could argue for formation in a loose association through turbulence rather than a compact cluster feeding competitive accretion.

Some relatively advanced young stars ($\sim$10^6 yr of age) have been seen in isolation but it is not known whether they have formed *in situ* or if they have drifted from their place of birth (Feigelson 1996; Contreras Peña et al. 2014). While 'isolated' young stars have been reported in the past, they are associated with large molecular clouds (Grinin et al. 1991; The, de Winter & Perez 1994), while the object reported herein is truly isolated; the observational limits on the proper motion and limited lifetime of this phase of formation mean that it must have formed within 1° of its present location on the sky.

4.5 Summary of interpretations

YSO outbursts are the only class of variable that explains the presence of warm, non-expanding dust local to the system, absence of a progenitor in deep optical and IR imaging prior to outburst, X-ray emission, extremely long duration of the transient event, and outflow velocities of the order of several hundred km s^{-1} in a Galactic object. The presence of a non-expanding cloud of warm dust is naturally explained by a YSO, but is difficult to explain with a nova interpretation, as any scenario involving the white dwarf as the source of the dust must have an expanding dust cloud in order to conceal the donor star, while any donor star capable of producing dust is impossible to reconcile with an absence in pre-outburst imaging without placing the system far beyond the Galactic bulge.

It is also possible that CX330 is the first in a new class of object unrepresented by the cases outlined above.

5 DISCUSSION

The most extreme observed YSO outbursts are known as FUor stars. All known FUors are located in star-forming regions (Hartmann & Kenyon 1987; Bell et al. 1995). Only 8–10 FUors have been observed to go into outburst, and efforts to search for YSO outbursts outside of star-forming regions have so far found that these outbursts are concentrated in star-forming regions (Contreras Peña et al. 2014). In large YSO outbursts such as these, it is common to not see photospheric lines as the star's photosphere is several magnitudes fainter than the continuum emission during the outburst.

Simulations of SF processes focus primarily on environments associated with GMC because most of the gas in the galaxy is in such clouds (>80 per cent in clouds with $M > 10^5$ M$_\odot$) (Stark & Lee 2006). SF theories can be grouped into two camps: hierarchical SF and clustered SF. In clustered SF, high-mass stars are formed through competitive accretion only in regions of very high density, with birth masses lower than the typical stellar mass and increased though accretion of unbound gas in the environment (Bonnell et al. 2001; Lada & Lada 2003). Hierarchical SF posits that stars form in a fractal distribution on a smoothly varying range of scales dominated by turbulence rather than magnetic support (Larson 1994; Bastian et al. 2007). There is evidence of hierarchical SF as a result of supernovae shocks (Oey et al. 2005) and in at least one association of massive stars in a larger SF region (Wright et al. 2014). If SF proceeds in a fractal distribution of scales, some few stars should be observed to form even in total isolation from the cloud complexes which have been the focus of large SF studies.

There are observational characteristics of CX330 that deviate from known YSO outbursts. Two IR spectra taken in 2014 and 2015 show no sign of CO $v' - v''$ 2–0 or 3–1 bands in either absorption or emission at 2.3 μm. CO in absorption is a defining marker of FUor variables, and is common in low-mass YSOs in either absorption or emission (Scoville et al. 1979; Krotkov, Wang & Scoville 1980). It is important to note that CO is destroyed at temperatures above 5000 K and collisional excitation requires that the temperature and density be above critical values of 3000 K and 10^{10} cm^{-3}, respectively (Scoville, Krotkov & Wang 1980). Additionally, the outflow speeds observed are unprecedented among outbursting YSOs, which typically have an outflow speed $\lesssim$300 km s^{-1}. Both of these differences can be explained if the gravitational potential is deeper than in previously observed outbursting YSOs. A forming YSO is larger than a main-sequence star of the same mass. The main-sequence structure of a star with an escape velocity of 700 km s^{-1} is therefore a rough lower limit on the mass of CX330, which is approximately 1.5 M$_\odot$ (Padmanabhan 2001).

Typical YSOs with large outbursts have a reflection nebula visible in the optical or NIR from the light reflecting off the surrounding molecular cloud. CX330 has no such reflection nebula, likely because it is not embedded in a molecular cloud of sufficient mass or size to have been detected in optical images. The mid-IR excess of CX330 that only appears after outburst is consistent with the reprocessing of optical light by a dusty envelope in YSOs, so it is likely that there is an extended local structure of dust and gas that is feeding the accretion in CX330. Indeed, the SED (Fig. 2) is consistent with class I/II YSOs.

YSOs undergoing extreme accretion disc instability episodes such as FUor types are young enough (<10^6 yr) that a large molecular cloud would not have had time to disperse (Blaauw 1964). This

indicates that the cloud collapse for CX330 was rapid, favouring turbulent formation scenarios hinging upon the Jean's mass (Larson 1994). As stars undergoing such accretion events are expected to be very young and are predicted to be a repeated but rare phase in most YSO development tracks, this discovery may force a revision of our understanding of typical SF environments. Using the large IR outbursts to find new outbursting YSOs offers a new window into SF theories by sampling a dramatically different phase space of formation conditions than is present in large star-forming regions (Contreras Peña et al. 2014).

ACKNOWLEDGEMENTS

TJM thanks Rob Fender, Selma de Mink, and Anna Scaife for discussions. CTB, TJM, and JDG thank Neal Evans for useful discussions. CTB thanks Paul Sell for discussions on emission from shocks. CTB, TJM, and LC thank Ulisse Munari for insights on the optical spectral properties. RIH acknowledges support from the National Science Foundation under Grant No. AST-0 908789. PGJ and MAPT acknowledge support from the Netherlands Organisation for Scientific Research. This research has made use of NASA's Astrophysics Data System Bibliographic Services and of SAOImage DS9, developed by Smithsonian Astrophysical Observatory.

REFERENCES

André P. et al., 2010, A&A, 518, L102
Ashok N. M., Banerjee D. P. K., 2003, A&A, 409, 1007
Bastian N., Ercolano B., Gieles M., Rosolowsky E., Scheepmaker R. A., Gutermuth R., Efremov Y., 2007, MNRAS, 379, 1302
Bell K. R., Lin D. N. C., Hartmann L. W., Kenyon S. J., 1995, ApJ, 444, 376
Benjamin R. A. et al., 2003, PASP, 115, 953
Blaauw A., 1964, ARA&A, 2, 213
Bonnell I., Bastien P., 1992, ApJ, 401, L31
Bonnell I. A., Bate M. R., Clarke C. J., Pringle J. E., 2001, MNRAS, 323, 785
Britt C. T. et al., 2014, ApJS, 214, 10
Cardelli J. A., Clayton G. C., Mathis J. S., 1989, ApJ, 345, 245
Carey S. J. et al., 2009, PASP, 121, 76
Chesneau O. et al., 2008, A&A, 487, 223
Churchwell E. et al., 2009, PASP, 121, 213
Contreras Peña C. et al., 2014, MNRAS, 439, 1829
Contreras Peña C. et al., 2016a, MNRAS, preprint (arXiv:1602.06269)
Contreras Peña C. et al., 2016b, MNRAS, preprint (arXiv:1602.06267)
Das R. K., Banerjee D. P. K., Ashok N. M., Chesneau O., 2008, MNRAS, 391, 1874
Elmegreen B. G., 2000, ApJ, 530, 277
Esenoglu H. H., Saygac A. T., Bianchini A., Retter A., Özkan M. T., Altan M., 2000, A&A, 364, 191
,Evans N. J., II et al., 2009, ApJS, 181, 321
Feigelson E. D., 1996, ApJ, 468, 306
Garmire G. P., 1997, BAAS, 29, 823
Gehrz R. D., Truran J. W., Williams R. E., Starrfield S., 1998, PASP, 110, 3
Gonzalez O. A., Rejkuba M., Zoccali M., Valenti E., Minniti D., Schultheis M., Tobar R., Chen B., 2012, A&A, 543, A13
González-Solares E. A. et al., 2008, MNRAS, 388, 89
Greiss S., Steeghs D. T. H., Jonker P. G., Torres M. A. P., Maccarone T. J., Hynes R. I., Britt C. T., 2014, MNRAS, 438, 2839
Grinin V. P., Kiselev N. N., Chernova G. P., Minikulov N. K., Voshchinnikov N. V., 1991, Ap&SS, 186, 283
Hachisu I., Kato M., 2014, ApJ, 785, 97
Hartmann L., 1998, Accretion Processes in Star Formation. Cambridge Univ. Press, Cambridge
Hartmann L., Kenyon S. J., 1987, ApJ, 312, 243
Hartmann L., Kenyon S. J., 1996, ARA&A, 34, 207
Herbig G. H., 1977, ApJ, 217, 693
Hong J., van den Berg M., Schlegel E. M., Grindlay J. E., Koenig X., Laycock S., Zhao P., 2005, ApJ, 635, 907
Jonker P. G. et al., 2011, ApJS, 194, 18
Jonker P. G. et al., 2014, ApJS, 210, 18
Kenyon S. J., Hartmann L. W., 1991, ApJ, 383, 664
Koenig X. P., Leisawitz D. T., 2014, ApJ, 791, 131
Krotkov R., Wang D., Scoville N. Z., 1980, ApJ, 240, 940
Lada C. J., Lada E. A., 2003, ARA&A, 41, 57
Larson R. B., 1994, in Clemens D. P., Barvainis R., eds, ASP Conf. Ser. Vol. 65, Clouds, Cores, and Low Mass Stars. Astron. Soc. Pac., San Francisco, p. 125
Livio M., 1999, Phys. Rep., 311, 225
Miller A. A. et al., 2011, ApJ, 730, 80
Minniti D. et al., 2010, New Astron., 15, 433
Munari U., Dallaporta S., Castellani F., Valisa P., Frigo A., Chomiuk L., Ribeiro V. A. R. M., 2013, MNRAS, 435, 771
Munari U., Mason E., Valisa P., 2014, A&A, 564, A76
Naito H. et al., 2012, A&A, 543, A86
Oey M. S., Watson A. M., Kern K., Walth G. L., 2005, AJ, 129, 393
Osterbrock D. E., 1989, Astrophysics of Gaseous Nebulae and Active Galactic Nuclei. University Science Books, Mill Valley, CA
Padmanabhan T., 2001, Theoretical Astrophysics - Volume 2, Stars and Stellar Systems. Cambridge Univ. Press, Cambridge
Pejcha O., 2009, ApJ, 701, L119
Planck Collaboration XIII, 2014, A&A, 571, A13
Qiu K. et al., 2008, ApJ, 685, 1005
Raj A. et al., 2015, AJ, 149, 136
Rieke G. H. et al., 2004, ApJS, 154, 25
Robitaille T. P., Whitney B. A., Indebetouw R., Wood K., 2007, ApJS, 169, 328
Robitaille T. P. et al., 2008, AJ, 136, 2413
Sandell G., Weintraub D. A., 2001, ApJS, 134, 115
Scoville N. Z., Hall D. N. B., Ridgway S. T., Kleinmann S. G., 1979, ApJ, 232, L121
Scoville N. Z., Krotkov R., Wang D., 1980, ApJ, 240, 929
Seaton M. J., 1979, MNRAS, 187, 73p
Skinner S. L., Güdel M., Briggs K. R., Lamzin S. A., 2010, ApJ, 722, 1654
Skrutskie M. F. et al., 2006, AJ, 131, 1163
Stark A. A., Lee Y., 2006, ApJ, 641, L113
Steele M. M., Zepf S. E., Kundu A., Maccarone T. J., Rhode K. L., Salzer J. J., 2011, ApJ, 739, 95
Strope R. J., Schaefer B. E., Henden A. A., 2010, AJ, 140, 34
The P. S., de Winter D., Perez M. R., 1994, A&AS, 104, 315
Tylenda R. et al., 2011, A&A, 528, A114
Udalski A., Szymanski M. K., Soszynski I., Poleski R., 2008, Acta Astron., 58, 69
Udalski A. et al., 2012, Acta Astron., 62, 133
Udalski A., Szymański M. K., Szymański G., 2015, Acta Astron., 65, 1
Warner B., 2003, Cataclysmic Variable Stars. Cambridge Univ. Press, Cambridge
Wevers T. et al., 2016, MNRAS, 458, 4530
Williams S. C., Bode M. F., Darnley M. J., Evans A., Zubko V., Shafter A. W., 2013, ApJ, 777, L32
Woudt P. A., Steeghs D., 2005, in Hameury J.-M., Lasota J.-P., eds, ASP Conf. Ser. Vol. 330, The Astrophysics of Cataclysmic Variables and Related Objects. Astron. Soc. Pac., San Francisco, p. 451
Wright E. L. et al., 2010, AJ, 140, 1868
Wright N. J., Parker R. J., Goodwin S. P., Drake J. J., 2014, MNRAS, 438, 639
Yaron O., Prialnik D., Shara M. M., Kovetz A., 2005, ApJ, 623, 398

This paper has been typeset from a TEX/LATEX file prepared by the author.